Simulation of many-body localization and time crystals in two dimensions with the neighborhood tensor update

Jacek Dziarmaga [*]

Institute of Theoretical Physics, Jagiellonian University, ulica Łojasiewicza 11, 30-348 Kraków, Poland

The Heisenberg antiferromagnet with discrete disorder on an infinite square lattice is evolved in time from an initial Néel state. The simulation is performed with the neighborhood tensor update algorithm for an infinite projected entangled pair state [Dziarmaga, Phys. Rev. B **104**, 094411 (2021)]. Ancillary spins are used to average over two or five discrete values of disorder. With a bond dimension up to 20, evolution times are long enough to identify a many-body localized regime for a strong enough disorder. Furthermore, the same Hamiltonian is subject to periodic spin flips. Simulations of the Floquet dynamics show that it can sustain a time crystalline stage for a strong enough disorder.

I. INTRODUCTION

Weakly entangled quantum states can be represented efficiently by tensor networks [1,2], including the one-dimensional (1D) matrix product state (MPS) [3], its two-dimensional (2D) generalization known as a projected entangled pair state (PEPS) [4,5], and a multiscale entanglement renormalization ansatz [6–9]. The MPS ansatz provides a compact representation of ground states of 1D gapped local Hamiltonians [1,10,11] and purifications of their thermal states [12]. It is also the ansatz underlying the density matrix renormalization group (DMRG) [13–16]. Analogously, the 2D PEPS is expected to represent ground states of 2D gapped local Hamiltonians [1,2] and their thermal states [17,18], although representability of area-law states, in general, was shown to have its limitations [19]. As a variational ansatz tensor networks do not suffer from the sign problem plaguing the quantum Monte Carlo. Consequently, they can deal with fermionic systems [20–24], as was shown for both finite [25] and infinite PEPS (iPEPS) [26,27].

The PEPS was originally proposed as an ansatz for ground states of finite systems [28,29], generalizing earlier attempts to construct trial wave functions for specific models [4]. The subsequent development of efficient numerical methods for an iPEPS [30–33], shown in Fig. 1(a), promoted it as one of the methods of choice for strongly correlated systems in two dimensions. Its power was demonstrated, e.g., by a solution of the long-standing magnetization plateaus problem in the highly frustrated compound $SrCu_2(BO_3)_2$ [34,35], establishing the striped nature of the ground state of the doped 2D Hubbard model [36], and new evidence supporting a gapless spin liquid in the kagome Heisenberg antiferromagnet [37]. Recent developments in iPEPS optimization [38–40], contraction [41,42], energy extrapolations [43], and universality-class estimation [44–46] pave the way towards even more complicated problems, including simulation of thermal states

[47–61], mixed states of open systems [55,62,63], excited states [64,65], and real-time evolution [55,66–73]. In parallel with iPEPS, there is continuous progress in simulating systems on cylinders of finite width using DMRG. This numerically highly stable method that is now routinely used to investigate 2D ground states [36,74] was applied also to thermal states on a cylinder [75–79]. However, the exponential growth of the bond dimension limits the cylinder's width to a few lattice sites. Among alternative approaches are direct contraction and renormalization of a three-dimensional tensor network representing a 2D thermal density matrix [80–87] and a cluster expansion [88].

In this paper we apply the recently defined neighborhood tensor update (NTU) algorithm [71,72] to simulate unitary time evolution of a 2D many-body localizing (MBL) system: the antiferromagnetic spin-1/2 Heisenberg model with discrete disorder initialized in the Néel state. The same simulations were performed previously [66,69] with the full update (FU) and simple update (SU) algorithms. NTU was intended as a reasonable trade-off between FU and SU which is more accurate than SU but, at the same time, more efficient and stable than FU. The efficiency allows us to reach bond dimensions up to 20 that in turn permit longer evolution times. The longer evolution enables a more reliable identification of a MBL regime for strong enough disorder. Encouraged by this quantitative progress, we supplement the model with periodic spin flips. This Floquet dynamics was previously simulated with SU [70]. Here we obtain long enough evolution times, converged in the bond dimension, to identify time crystals for strong enough disorder.

This paper is organized as follows. In Sec. II we overview the NTU algorithm, whose more technical details can be found in the Appendix. The applications to many-body localization and time crystals follow in Secs. III and IV, respectively. We conclude in Sec. V.

II. NEIGHBORHOOD TENSOR UPDATE

In the following NTU simulations we use the second-order Suzuki-Trotter decomposition of small time steps. An application of a two-site nearest-neighbor (NN) Trotter gate is
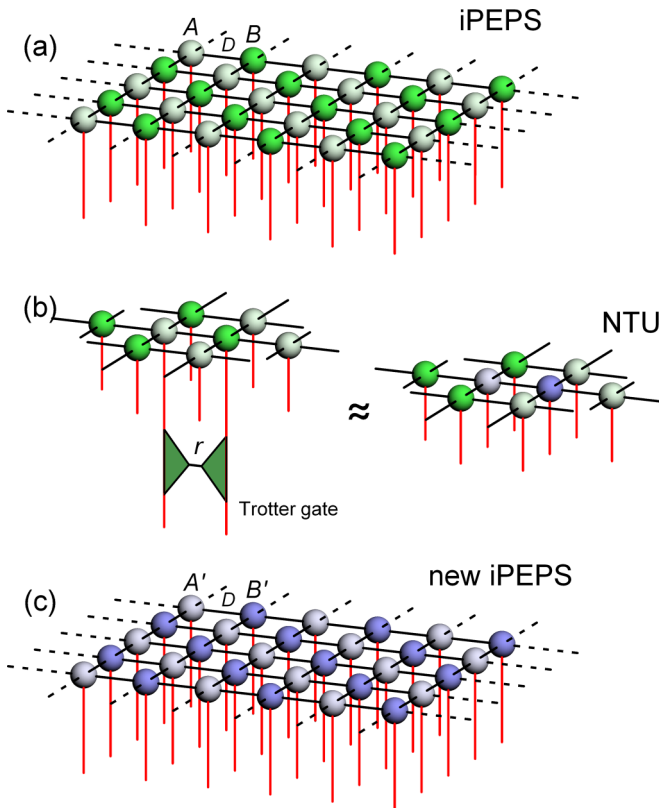
---
[*]dziarmaga@th.if.uj.edu.pl

FIG. 1. Essential NTU. (a) Infinite PEPS with tensors A (lighter green) and B (darker green) on the two sublattices. The red lines are physical spin indices, and the black lines are bond indices, with bond dimension D, contracting NN sites. In one of the Suzuki-Trotter steps a Trotter gate is applied to every horizontal NN pair of A-B tensors (but not to horizontal B-A pairs). The gate can be represented as a contraction of two tensors by an index with dimension r. When the two tensors are absorbed into tensors A and B, the bond dimension between them increases from D to $r \times D$. (b) The A-B pair—with a Trotter gate applied to it—is approximated by a pair of new tensors, A' (lighter blue) and B' (darker blue), connected by an index with the original dimension D, see (c). The new tensors are optimized to minimize the Frobenius norm of the difference between the two networks in (b). The networks surround the considered NN bond with its six NN tensors. They provide a minimal tensor environment (necessary to make efficient use of limited D) which can be contracted exactly in an efficient way. After A' and B' are converged, they replace all tensors A and B in a new iPEPS. Then the next Trotter gate can be applied. More details of the NTU algorithm can be found in the Appendix.

explained in diagrammatic form in Fig. 1. NTU is intermediate between the two most popular simulation schemes: the SU and FU [55]. In both after a Trotter gate is applied to a pair of NN sites a bond dimension of the index between the sites is increased by a factor equal to the singular value decomposition (SVD) rank of the gate. In order to prevent its exponential growth with time the dimension is truncated to a predefined value, D, in a way that minimizes error incurred by the truncation. The two schemes differ by a measure of the error: FU takes into account the full infinite tensor environment, while SU takes into account only the bonds adjacent to the NN sites. The former is expected to perform better

in the case of long-range correlations, while the latter is, at least formally, more efficient thanks to its locality, although it makes less efficient use of the limited bond dimension than FU. In NTU the error measure is induced by the sites that are NN to the Trotter gate. It was demonstrated [71] that in practice it compromises the FU accuracy only a little for the price of small numerical overhead over SU; hence, it may turn out to be an optimal trade-off for many applications, especially when quantum correlations are not exceedingly long like in, e.g., Kibble-Zurek quenches in two dimensions [72]. In this sense it seems to be tailored for time evolution of MBL systems where the localization is expected to limit the growth of correlations.

NTU can be placed in a broader context by noting that it is a special case of a cluster update [89] in which the size of the tensor environment is a variable parameter interpolating between a local environment in SU and an infinite one in FU. In the case of ground state calculations the cluster update was thoroughly investigated in Refs. [90,91], where the interplay between maximal achievable correlation length and the cluster size was demonstrated. In NTU the cluster includes only the neighboring sites (see Fig. 1) to allow the error measure to be calculated exactly but with little numerical overhead over SU. The calculation involves only tensor contractions that are fully parallelizable. Its exactness warrants the error measure being a manifestly Hermitian and non-negative quadratic form. This property is essential for the stability of NTU and makes it distinct from FU, where an approximate corner transfer matrix renormalization [2,33] often breaks the Hermiticity and non-negativeness. In the case of longer correlations the small environment can, admittedly, make NTU converge with the bond dimension more slowly than FU, but this can often be compensated by its better numerical efficiency and stability, which allow NTU to reach higher bond dimensions [71].

III. MANY-BODY LOCALIZATION

When excited, the MBL systems evade thermalization but retain memory of their initial conditions [92,93]. The memory is sustained by localization that gives rise to quasilocal constants of motion [94–96] that allow the evolving state to equilibrate, but to a nonthermal stationary state. In two dimensions, which is harder to investigate by any means (analytic, numerical, or experimental [97]), the issue is far from settled. The 2D MBL was suggested to be unstable towards a crossover to ergodicity on very long timescales [98]. Several numerical approaches were proposed to address the 2D problem [66,69,99–104]. This paper follows the approach of simulating the time evolution of a 2D MBL system with the iPEPS tensor network [66,69,101,103,104], but it employs the NTU algorithm [71]. For a localizing system this algorithm is expected to offer an optimal combination of stability and efficiency.

In order to be more specific, we consider the antiferromagnetic Heisenberg model with disorder on an infinite square lattice:

$$H = \sum_{\langle j, j' \rangle} \vec{S}_j \vec{S}_{j'} + \sum_j h_j S_j^z. \tag{1}$$
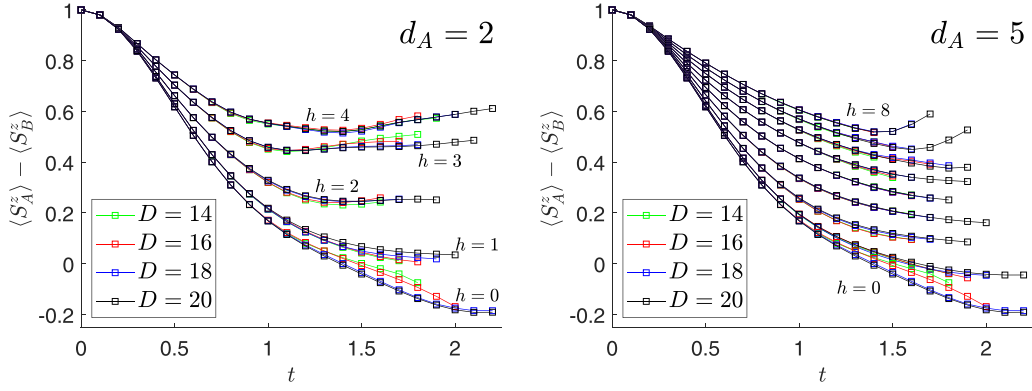
FIG. 2. Many-body localization. A spin imbalance as a function of time for different disorder strengths h and ancillary dimensions d_A. Here the many-body localizing Hamiltonian (2) was initialized with the Néel state of spins (3). For $d_A = 2$ and 5 we show $h = 0, 1, \ldots, 4$ and $h = 0, 1, \ldots, 8$, respectively. The time step $dt = 0.01$, and the evolution is terminated when the Trotter gate error (A5) exceeds $\delta = 0.03$ for the first time.

Here $\vec{S}_j = \frac{1}{2}\vec{\sigma}_j$ is a spin-1/2 operator at site j. Every random h_j is drawn independently from a set of d_A evenly spaced discrete values in an interval $[-h, h]$. For instance, $h_j \in \{-h, h\}$ for $d_A = 2$, $h_j \in \{-h, 0, h\}$ for $d_A = 3$, etc. The Hamiltonian is initialized with a Néel state $|\text{Néel}\rangle$ with spins pointing up (down) along the z axis on sublattice A (B) of an infinite checkerboard lattice. This initial product state is evolved in time. Expectation values of spin operators at time t are averaged over all possible realizations of the disorder.

Here, as in Refs. [66,69,103,104], an equivalent formulation of the problem is considered:

$$H_{\text{MBL}} = \sum_{\langle j, j' \rangle} \vec{S}_j \vec{S}_{j'} + \frac{h}{S} \sum_j A_j^z S_j^z, \quad (2)$$

where A_j^z is an ancilla spin-S operator at site j that takes $d_A = 2S + 1$ evenly spaced discrete values in an interval $[-S, S]$. In this formulation the initial state is replaced by an equivalent uniform product:

$$|\psi(0)\rangle = |\text{Néel}\rangle \prod_j |+\rangle_j, \quad (3)$$

where j runs over ancillas. Every ancillary spin S is prepared in a superposition:

$$|+\rangle_j = (2S + 1)^{-1/2} \sum_{m_j=-S}^{S} |m_j\rangle, \quad (4)$$

with the same probability for all evenly spaced values of disorder $h_j = m_j h / S \in [-h, h]$. The two formulations are equivalent in the sense that a disorder-averaged expectation value of any operator $\mathcal{O}$ at time t in the former is equal to $\langle \psi(t)|\mathcal{O}|\psi(t)\rangle$ in the latter.

The Hamiltonian (2) is the same as in Ref. [69], and the same ancillary dimensions $d_A = 2$ and 5 are considered for a range of disorder strengths. Unlike Ref. [69] NTU is employed instead of SU, and bond dimensions up to $D = 20$ are reached instead of $D = 4, 5$. As a result NTU evolution times are long enough to reach some semiquantitative conclusions without any extrapolation in time.

Figure 2 shows the time evolution of spin imbalance between sublattices A and B, $\langle \psi(t)|S_A^z|\psi(t)\rangle - \langle \psi(t)|S_B^z|\psi(t)\rangle$, as a function of evolution time t for several values of disorder strength h. In particular both panels show the evolution without disorder, $h = 0$, when the imbalance crosses from positive to negative. Not quite surprisingly, in the absence of MBL this simulation becomes poorly converged in D when the system begins to thermalize, and growing entanglement becomes difficult to accommodate with the tensor network. The same comment, although to a lesser extent, applies to a finite, but weak, disorder with $h = 1$. For higher disorder strengths the difference between $d_A = 2$ and $d_A = 5$ appears to be rather quantitative. In the former case, as far as the limited evolution time permits us to conclude, there seems to be a crossover to MBL between $h = 1$ and $h = 2$. For $h \geqslant 2$ the spin imbalance at first goes down from the initial value of 1 before it bounces up. The memory of the initial spin imbalance between the sublattices is not lost. In the case of $d_A = 5$ a similar bounce up is observed, within the available evolution time, for only the highest disorder strengths $h = 7, 8$. For $h = 2, \ldots, 6$ the NTU evolution terminates before bouncing up. It remains an open question whether the spin imbalance is bouncing up at later times or the evolution is heading straight towards thermalization and how precisely it depends on h. For the available evolution times we can crudely estimate the crossover between the (hypothetical) thermalization and MBL takes place between $h = 1$ and $h = 7$.

It is worth emphasizing that, thanks to NTU (instead of SU) and bond dimensions up to $D = 20$ (instead of $D = 4, 5$), our (D-converged) evolution times are typically twice as long as in Ref. [69]. This allows us to identify the MBL regime not only for $d_A = 5$ but also for the two-level disorder.

In the next section the same Hamiltonian (2) is promoted to a Floquet Hamiltonian by the action of time-periodic spin flips.

IV. TIME CRYSTALS

Time crystals were, at first, envisioned by Wilczek as spontaneous time translation symmetry breaking in a ground state of a quantum Hamiltonian [105], but this original idea was proved wrong by a no-go theorem [106,107]. More recently,
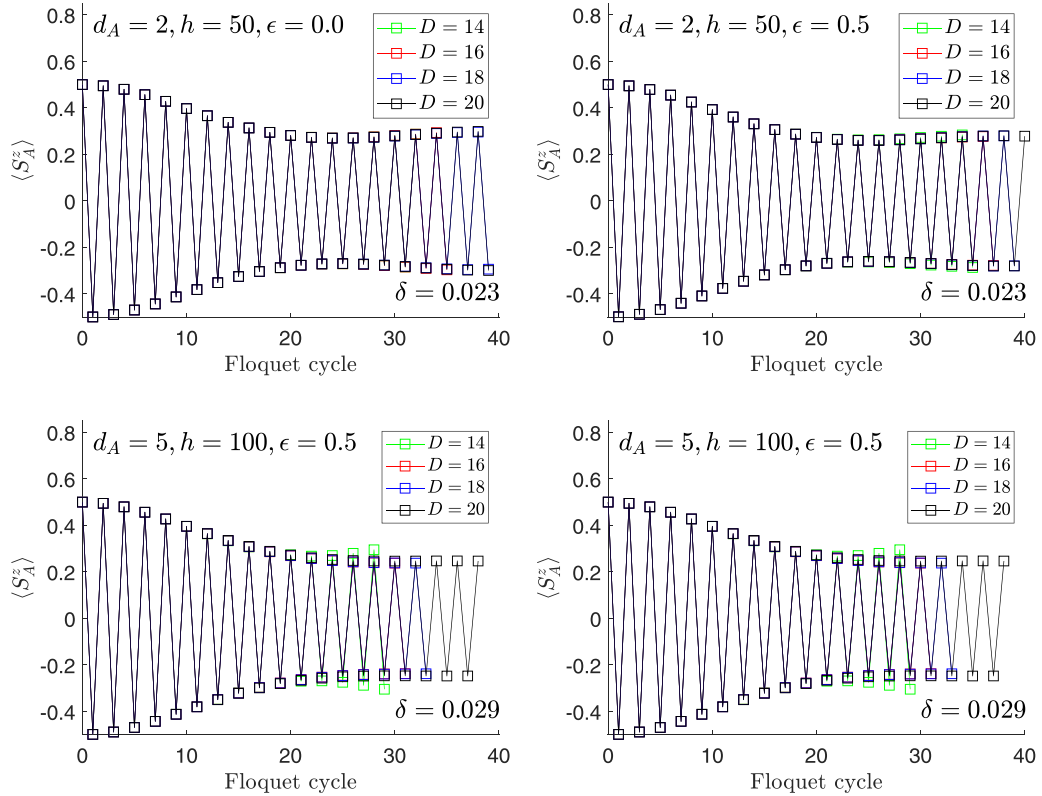
FIG. 3. Time crystallization. A stroboscopic time evolution of magnetization on sublattice A as a function of the number of cycles for two combinations (d_A, h) of the ancillary dimension and disorder strength, (2,50) and (5,100), and two values of the angle deficit parameter: $\epsilon = 0$ and 0.5. Here the Floquet Hamiltonian (5) with period $T = 0.1$ was initialized with a Néel state of spins along S^z (3). The time step was $dt = 0.001$, and the evolution was terminated when the Trotter gate error δ, defined in (A5), exceeded for the first time the value in the bottom right corner of each panel. In the top and bottom right panels this value is chosen such that the results for $D = 18, 20$ appear converged until the termination. In the bottom left case there is still some dependence on D with a tendency to improve the time crystal with increasing D.

spontaneous discrete time translation symmetry breaking was demonstrated [108–111] in Floquet systems that are periodic in time. These ideas inspired experiments that were performed on a variety of physical platforms [112–119]. The fast-growing field is already the subject of several reviews [120–122]. A few mechanisms have been proposed to help a Floquet system avoid heating. They include the many-body localization [123–125], prethermalization [126–128], and many-body quantum scars [129–132].

Here, as in Ref. [70], the MBL mechanism is considered. The Floquet Hamiltonian with period T is

$$H_F = \begin{cases} H_{MBL} & \text{when } t \in [0, T/2), \\ H_f & \text{when } t \in [T/2, T). \end{cases} \quad (5)$$

Here H_{MBL} is the same as in (2), and

$$H_f = (2\pi/T - 2\epsilon) \sum_j S_j^x. \quad (6)$$

For $\epsilon = 0$ its evolution operator $e^{-iH_f T/2}$ is a perfect spin-flip operator that is applied once per every period T. In general it is an imperfect spin rotation with an angle deficit ϵT. The initial state is again the Néel state in (3).

Figure 3 shows examples of stroboscopic time evolutions for ancillary dimensions $d_A = 2, 5$ and the corresponding disorder strengths $h = 50, 100$ that turn out to be strong enough to stabilize an unambiguous time crystalline stage. Figure 3 also demonstrates the robustness of these time crystals against the spin-flip imperfection with $\epsilon = 0.5$. On the other hand, when the disorder is not strong enough, the time crystalline stage either cannot be identified at all or disappears within the achievable evolution time (see the left and right panels in Fig. 4, respectively). The disappearance is accompanied by a worsening convergence with D, as might have been expected when MBL is not effective enough.

V. CONCLUSION

The neighborhood tensor update algorithm [71] was employed to simulate unitary time evolution of the square-lattice antiferromagnetic spin-1/2 Heisenberg model with discrete disorder. Starting from the Néel state many-body localized regimes were identified—for both the two-level and five-level disorders—where the system retains some memory of the initial state. When promoted to a Floquet Hamiltonian with periodic (imperfect) spin flips the simulations revealed extended time crystalline stages for strong enough disorder.
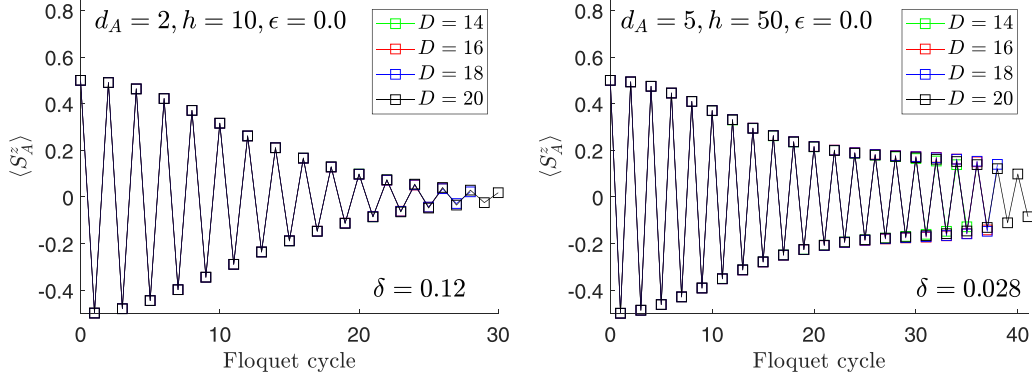
FIG. 4. Time crystallization failure. Two generic examples of stroboscopic time evolution where the disorder is too weak to sustain a time crystal (TC) that extends beyond the achievable simulation time. In the left panel the TC cannot be identified at all, while in the right one there seems to be a transient TC stage that begins to disappear after around 40 Floquet cycles. Here the Floquet Hamiltonian (5) with period $T = 0.1$ was initialized with the Néel state of spins (3). The time step was $dt = 0.001$, and the evolution was terminated when the Trotter gate error δ, defined in (A5), exceeded for the first time the value in the bottom right corner of each panel.

ACKNOWLEDGMENTS

APPENDIX: ALGORITHM

The core of the NTU scheme [71] is outlined in Figs. 1, 5–7. Figure 5 shows the application of a two-site Trotter gate to a pair of NN iPEPS tensors, A and B. The rank-r gate enlarges the bond dimension from D to Dr, which has to be truncated back to D in an optimal way. For the sake of efficiency, a QR decomposition introduces reduced matrices R_A and R_B in place of full tensors [133]. A SVD of their product, $R_A R_B^T$, can be truncated to provide a preliminary truncation of the bond dimension. The truncated reduced matrices, M_A and M_B, are further optimized iteratively in Figs. 6 and 7. After convergence they are contracted again with the fixed isometries, Q_A and Q_B, into new iPEPS tensors A' and B'. The numerical cost of the procedures in Fig. 5 scales as D^5.

Further NTU optimization minimizes the difference between the left-hand side (LHS) and the right-hand side (RHS) of the equation in Fig. 1(b). The contraction $A' - B'$ on its RHS (the purple tensors) is the same contraction as in Fig. 5(e), and it has to be understood as the diagram in Fig. 5(d). In this way the RHS depends on the product of the matrices to be optimized: $M_A M_B^T$. Therefore, the norm squared of the difference between the LHS and the RHS can be written as

$$F\left(M_A M_B^T\right) = \left[M_A M_B^T - R_A R_B^T\right]^\dagger g\left[M_A M_B^T - R_A R_B^T\right], \quad (A1)$$

where g is the metric tensor constructed in Fig. 6. With metric g fixed, matrices M_A and M_B are optimized to make them the best approximation to the untruncated/exact product $R_A R_B^T$. For a fixed M_B the cost function (A1) becomes a quadratic form in M_A:

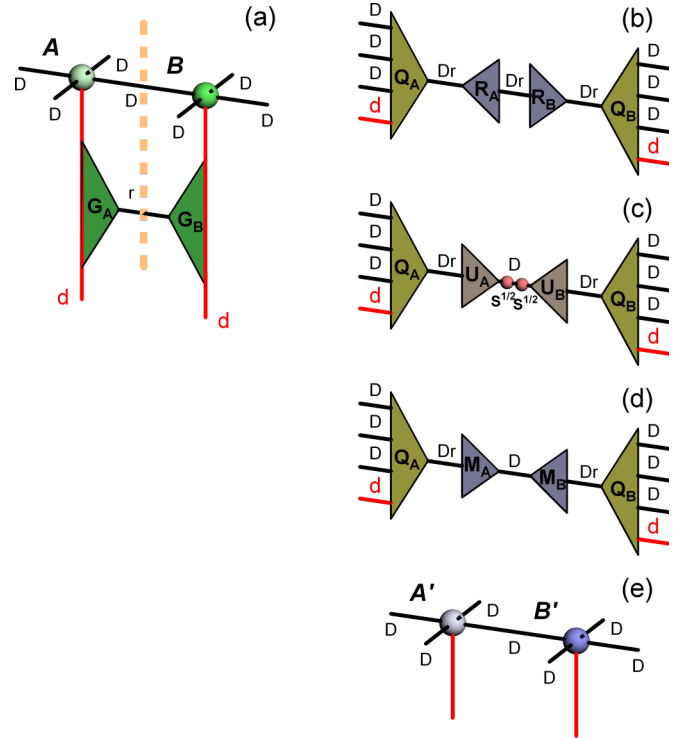$$F_A(M_A) = M_A^\dagger g_A M_A - M_A^\dagger J_A - J_A^\dagger M_A + F(0), \quad (A2)$$

FIG. 5. Trotter gate. (a) A two-site gate is applied to physical indices of NN tensors A and B as in Fig. 1(b). The gate is replaced by two tensors, G_A and G_B, contracted by an index with dimension r. (b) The tensor contraction AG_A is QR decomposed into $Q_A R_A$. Similarly, $BG_B = Q_B R_B$. Isometries $Q_{A,B}$ will remain fixed. (c) After SVD, $R_A R_B^T = U_A S U_B^T$, S is truncated to D, leading singular values. (d) Matrices $M_A = U_A S^{1/2}$ and $M_B = S^{1/2} U_B^T$ are made by absorbing a square root of truncated S symmetrically. (e) At this point new iPEPS tensors can be obtained as $A' = Q_A M_A$ and $B' = Q_B M_B$, ending the story. This scheme was referred to as an SVD update (SVDU) in Ref. [71]. In NTU scheme matrices $M_{A,B}$ are further optimized in the neighborhood tensor environment in Fig. 1 before being contracted back with the fixed isometries $Q_{A,B}$ to make new iPEPS tensors A' and B'.
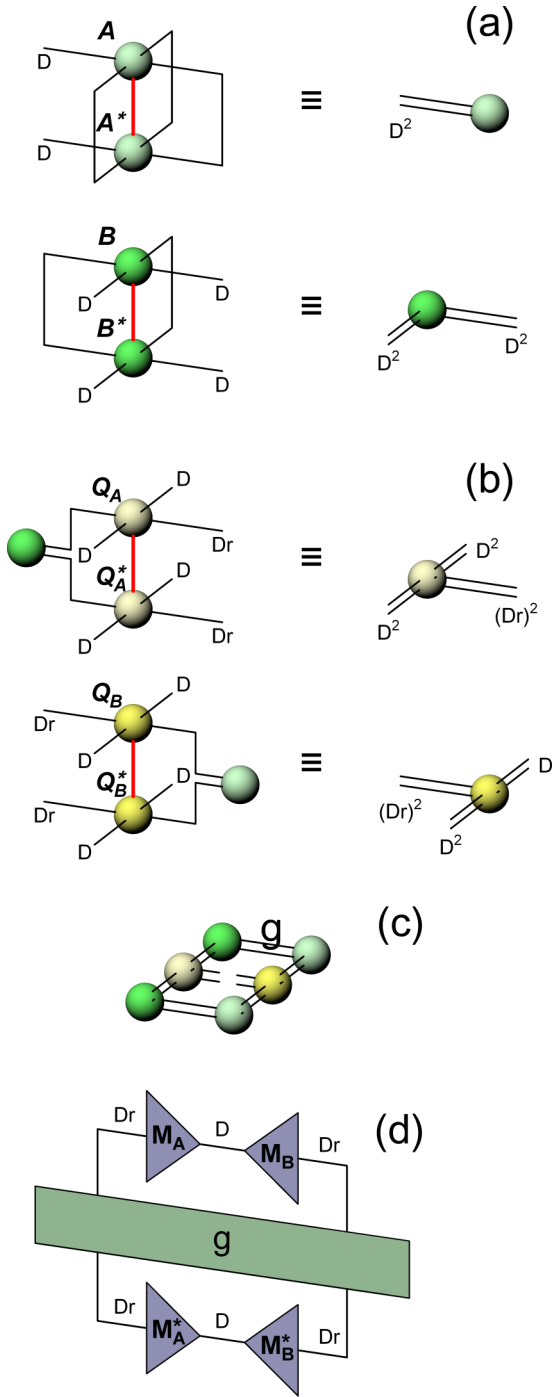
FIG. 6. Metric tensor. Norm squared of the matrix product, $||M_A M_B^T||^2$, is shown in (d). Here g is a metric tensor assembled in (c). The upper (lower) pair of free indices in (c) corresponds to the upper (lower) pair of indices of g in (d). (c) is assembled from six edge tensors, two examples of which are shown in (a), and two double isometric tensors, shown in (b). The cost of all the contractions scales as D^8 and is fully parallelizable.

where g_A and J_A depend on the fixed M_B [see Figs. 7(b) and 7(c)]. The matrix is optimized as

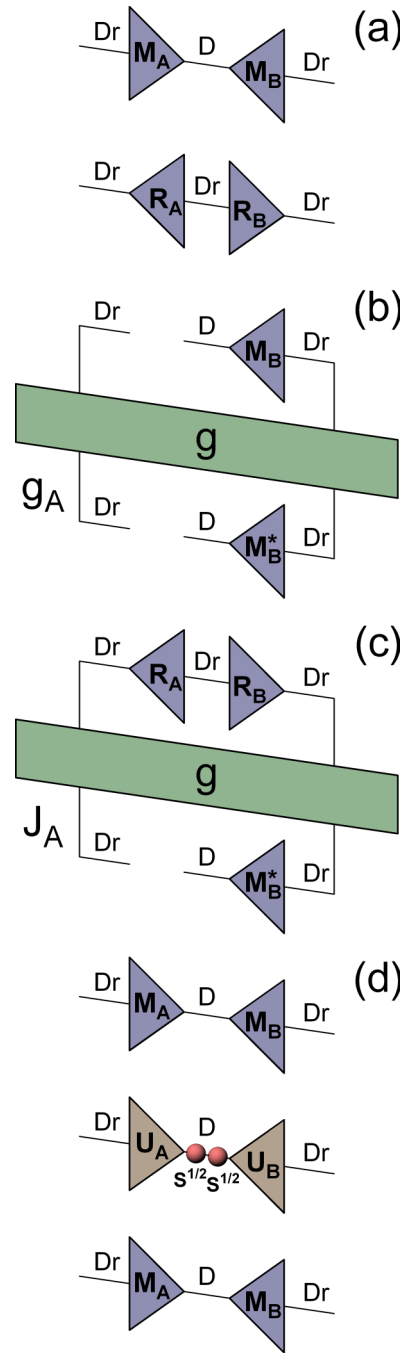$$M_A = \text{pinv}(g_A) J_A, \tag{A3}$$

FIG. 7. NTU optimization loop. (a) Matrices M_A and M_B are optimized for their product, $M_A M_B^T$, to be the best approximation to the exact product, $R_A R_B^T$. The error is measured with the metric in Fig. 6(d). (b) Reduced metric tensor g_A for matrix M_A. (c) Reduced source term J_A for matrix M_A. (d) A product of converged matrices is subject to a SVD, $M_A M_B = U_A S U_B^T$, after which new balanced matrices, $M_A = U_A S^{1/2}$ and $M_B^T = S^{1/2} U_B^T$, are formed by absorbing singular values S in a symmetric way. However, iterative optimization of the matrices is not symmetric. Before optimization with respect to M_A the matrices are "tilted" as $M_A = U_A S$ and $M_B^T = U_B^T$ and vice versa [133].

where tolerance of the pseudoinverse can be adjusted to minimize $F_A[\text{pinv}(g_A) J_A]$. Thanks to the exactness of g in NTU,

the optimal tolerance is usually in the range $10^{-12}, \ldots, 10^{-8}$. This optimization of M_A is followed by a similar optimization of M_B. The optimizations are repeated in a loop,

$$\rightarrow M_A \rightarrow M_B \rightarrow, \qquad \text{(A4)}$$

until convergence of a relative NTU error: $F(M_A M_B^T)/F(0)$. In general the converged error is nonzero due to the necessary truncation of the bond dimension.

The converged error is used as a criterion to terminate the time evolution. More specifically, we use

$$\delta = dt^{-1} \sqrt{F\left(M_A M_B^T\right)/F(0)} \qquad \text{(A5)}$$

to measure the accuracy of the Trotterized evolution. It should be independent of the time step for small enough dt. The

square root makes $dt\delta$ a rough estimator of a relative error of the wave function inflicted by the Trotter gate and, as such, also of an error of its expectation values. In the worst-case scenario, where the gate errors accumulate in an additive way, a typical relative error after time t is proportional to $t\delta$, where δ is averaged over the evolution time.

Except for SVD of small matrices, $R_A R_B^T$ and $M_A M_B^T$, the $\propto D^8$ operations, which are required to simulate time evolution in the NTU scheme, are fully parallelizable. A potential bottleneck is the calculation of expectation values that requires the corner transfer matrix renormalization group [2]. However, the expectation values usually do not need to be evaluated after every time step, and they may not require the same precision as stable evolution with the full update scheme.

[1] F. Verstraete, V. Murg, and J. Cirac, Adv. Phys. **57**, 143 (2008).

[2] R. Orús, Ann. Phys. (Amsterdam) **349**, 117 (2014).

[3] M. Fannes, B. Nachtergaele, and R. Werner, Commun. Math. Phys. **144**, 443 (1992).

[4] Y. Nishio, N. Maeshima, A. Gendiar, and T. Nishino, arXiv:cond-mat/0401115.

[5] F. Verstraete and J. I. Cirac, arXiv:cond-mat/0407066.

[6] G. Vidal, Phys. Rev. Lett. **99**, 220405 (2007).

[7] G. Vidal, Phys. Rev. Lett. **101**, 110501 (2008).

[8] G. Evenbly and G. Vidal, Phys. Rev. Lett. **112**, 220502 (2014).

[9] G. Evenbly and G. Vidal, Phys. Rev. B **89**, 235113 (2014).

[10] M. B. Hastings, J. Stat. Mech. (2007) P08024.

[11] N. Schuch, M. M. Wolf, F. Verstraete, and J. I. Cirac, Phys. Rev. Lett. **100**, 030504 (2008).

[12] T. Barthel, arXiv:1708.09349.

[13] S. R. White, Phys. Rev. Lett. **69**, 2863 (1992).

[14] S. R. White, Phys. Rev. B **48**, 10345 (1993).

[15] U. Schollwöck, Rev. Mod. Phys. **77**, 259 (2005).

[16] U. Schöllwock, Ann. Phys. (Amsterdam) **326**, 96 (2011).

[17] M. M. Wolf, F. Verstraete, M. B. Hastings, and J. I. Cirac, Phys. Rev. Lett. **100**, 070502 (2008).

[18] A. Molnar, N. Schuch, F. Verstraete, and J. I. Cirac, Phys. Rev. B **91**, 045138 (2015).

[19] Y. Ge and J. Eisert, New J. Phys. **18**, 083026 (2016).

[20] P. Corboz, G. Evenbly, F. Verstraete, and G. Vidal, Phys. Rev. A **81**, 010303(R) (2010).

[21] C. Pineda, T. Barthel, and J. Eisert, Phys. Rev. A **81**, 050303(R) (2010).

[22] P. Corboz and G. Vidal, Phys. Rev. B **80**, 165129 (2009).

[23] T. Barthel, C. Pineda, and J. Eisert, Phys. Rev. A **80**, 042333 (2009).

[24] Z.-C. Gu, F. Verstraete, and X.-G. Wen, arXiv:1004.2563.

[25] C. V. Kraus, N. Schuch, F. Verstraete, and J. I. Cirac, Phys. Rev. A **81**, 052338 (2010).

[26] P. Corboz, R. Orús, B. Bauer, and G. Vidal, Phys. Rev. B **81**, 165104 (2010).

[27] P. Corboz, S. R. White, G. Vidal, and M. Troyer, Phys. Rev. B **84**, 041108(R) (2011).

[28] F. Verstraete and J. I. Cirac, arXiv:cond-mat/0407066.

[29] V. Murg, F. Verstraete, and J. I. Cirac, Phys. Rev. A **75**, 033605 (2007).

[30] J. Jordan, R. Orús, G. Vidal, F. Verstraete, and J. I. Cirac, Phys. Rev. Lett. **101**, 250602 (2008).

[31] H. C. Jiang, Z. Y. Weng, and T. Xiang, Phys. Rev. Lett. **101**, 090603 (2008).

[32] Z.-C. Gu, M. Levin, and X.-G. Wen, Phys. Rev. B **78**, 205116 (2008).

[33] R. Orús and G. Vidal, Phys. Rev. B **80**, 094403 (2009).

[34] Y. H. Matsuda, N. Abe, S. Takeyama, H. Kageyama, P. Corboz, A. Honecker, S. R. Manmana, G. R. Foltin, K. P. Schmidt, and F. Mila, Phys. Rev. Lett. **111**, 137204 (2013).

[35] P. Corboz and F. Mila, Phys. Rev. Lett. **112**, 147203 (2014).

[36] B.-X. Zheng, C.-M. Chung, P. Corboz, G. Ehlers, M.-P. Qin, R. M. Noack, H. Shi, S. R. White, S. Zhang, and G. K.-L. Chan, Science **358**, 1155 (2017).

[37] H. J. Liao, Z. Y. Xie, J. Chen, Z. Y. Liu, H. D. Xie, R. Z. Huang, B. Normand, and T. Xiang, Phys. Rev. Lett. **118**, 137202 (2017).

[38] H. N. Phien, J. A. Bengua, H. D. Tuan, P. Corboz, and R. Orús, Phys. Rev. B **92**, 035142 (2015).

[39] P. Corboz, Phys. Rev. B **94**, 035133 (2016).

[40] L. Vanderstraeten, J. Haegeman, P. Corboz, and F. Verstraete, Phys. Rev. B **94**, 155123 (2016).

[41] M. T. Fishman, L. Vanderstraeten, V. Zauner-Stauber, J. Haegeman, and F. Verstraete, Phys. Rev. B **98**, 235148 (2018).

[42] Z. Y. Xie, H. J. Liao, R. Z. Huang, H. D. Xie, J. Chen, Z. Y. Liu, and T. Xiang, Phys. Rev. B **96**, 045128 (2017).

[43] P. Corboz, Phys. Rev. B **93**, 045116 (2016).

[44] P. Corboz, P. Czarnik, G. Kapteijns, and L. Tagliacozzo, Phys. Rev. X **8**, 031031 (2018).

[45] M. Rader and A. M. Läuchli, Phys. Rev. X **8**, 031030 (2018).

[46] M. M. Rams, P. Czarnik, and L. Cincio, Phys. Rev. X **8**, 041033 (2018).

[47] P. Czarnik, L. Cincio, and J. Dziarmaga, Phys. Rev. B **86**, 245101 (2012).

[48] P. Czarnik and J. Dziarmaga, Phys. Rev. B **90**, 035144 (2014).

[49] P. Czarnik and J. Dziarmaga, Phys. Rev. B **92**, 035120 (2015).

[50] P. Czarnik, J. Dziarmaga, and A. M. Oleś, Phys. Rev. B **93**, 184410 (2016).

[51] P. Czarnik and J. Dziarmaga, Phys. Rev. B **92**, 035152 (2015).

[52] P. Czarnik, M. M. Rams, and J. Dziarmaga, Phys. Rev. B **94**, 235142 (2016).

[53] P. Czarnik, J. Dziarmaga, and A. M. Oleś, Phys. Rev. B **96**, 014420 (2017).

[54] Y.-W. Dai, Q.-Q. Shi, S. Y. Cho, M. T. Batchelor, and H.-Q. Zhou, Phys. Rev. B **95**, 214409 (2017).

[55] P. Czarnik, J. Dziarmaga, and P. Corboz, Phys. Rev. B **99**, 035115 (2019).

[56] P. Czarnik and P. Corboz, Phys. Rev. B **99**, 245107 (2019).

[57] A. Kshetrimayum, M. Rizzi, J. Eisert, and R. Orús, Phys. Rev. Lett. **122**, 070502 (2019).

[58] P. Czarnik, A. Francuz, and J. Dziarmaga, Phys. Rev. B **100**, 165147 (2019).

[59] J. L. Jiménez, S. P. G. Crone, E. Fogh, M. E. Zayed, R. Lortz, E. Pomjakushina, K. Conder, A. M. Läuchli, L. Weber, S. Wessel, A. Honecker, B. Normand, C. Rüegg, P. Corboz, H. M. Rønnow, and F. Mila, Nature (London) **592**, 370 (2021).

[60] D. Poilblanc, M. Mambrini, and F. Alet, SciPost Phys. **10**, 019 (2021).

[61] P. Czarnik, M. M. Rams, P. Corboz, and J. Dziarmaga, Phys. Rev. B **103**, 075113 (2021).

[62] A. Kshetrimayum, H. Weimer, and R. Orús, Nat. Commun. **8**, 1291 (2017).

[63] C. Mc Keever and M. H. Szymańska, Phys. Rev. X **11**, 021035 (2021).

[64] L. Vanderstraeten, M. Mariën, F. Verstraete, and J. Haegeman, Phys. Rev. B **92**, 201111(R) (2015).

[65] B. Ponsioen and P. Corboz, Phys. Rev. B **101**, 195109 (2020).

[66] C. Hubig and J. I. Cirac, SciPost Phys. **6**, 31 (2019).

[67] C. Hubig, A. Bohrdt, M. Knap, F. Grusdt, and J. I. Cirac, SciPost Phys. **8**, 21 (2020).

[68] A. Abendschein and S. Capponi, Phys. Rev. Lett. **101**, 227201 (2008).

[69] A. Kshetrimayum, M. Goihl, and J. Eisert, Phys. Rev. B **102**, 235132 (2020).

[70] A. Kshetrimayum, M. Goihl, D. M. Kennes, and J. Eisert, Phys. Rev. B **103**, 224205 (2021).

[71] J. Dziarmaga, Phys. Rev. B **104**, 094411 (2021).

[72] M. Schmitt, M. M. Rams, J. Dziarmaga, M. Heyl, and W. H. Zurek, arXiv:2106.09046.

[73] R. Kaneko and I. Danshita, arXiv:2108.11051.

[74] L. Cincio and G. Vidal, Phys. Rev. Lett. **110**, 067208 (2013).

[75] B. Bruognolo, Z. Zhu, S. R. White, and E. M. Stoudenmire, arXiv:1705.05578.

[76] B.-B. Chen, L. Chen, Z. Chen, W. Li, and A. Weichselbaum, Phys. Rev. X **8**, 031082 (2018).

[77] L. Chen, D.-W. Qu, H. Li, B.-B. Chen, S.-S. Gong, J. von Delft, A. Weichselbaum, and W. Li, Phys. Rev. B **99**, 140404(R) (2019).

[78] H. Li, B.-B. Chen, Z. Chen, J. von Delft, A. Weichselbaum, and W. Li, Phys. Rev. B **100**, 045110 (2019).

[79] B.-B. Chen, C. Chen, Z. Chen, J. Cui, Y. Zhai, A. Weichselbaum, J. von Delft, Z. Y. Meng, and W. Li, Phys. Rev. B **103**, L041107 (2021).

[80] W. Li, S.-J. Ran, S.-S. Gong, Y. Zhao, B. Xi, F. Ye, and G. Su, Phys. Rev. Lett. **106**, 127202 (2011).

[81] Z. Y. Xie, J. Chen, M. P. Qin, J. W. Zhu, L. P. Yang, and T. Xiang, Phys. Rev. B **86**, 045139 (2012).

[82] S.-J. Ran, W. Li, B. Xi, Z. Zhang, and G. Su, Phys. Rev. B **86**, 134429 (2012).

[83] S.-J. Ran, B. Xi, T. Liu, and G. Su, Phys. Rev. B **88**, 064407 (2013).

[84] S.-J. Ran, W. Li, S.-S. Gong, A. Weichselbaum, J. von Delft, and G. Su, Phys. Rev. B **97**, 075146 (2018).

[85] C. Peng, S.-J. Ran, T. Liu, X. Chen, and G. Su, Phys. Rev. B **95**, 075140 (2017).

[86] X. Chen, S.-J. Ran, T. Liu, C. Peng, Y.-Z. Huang, and G. Su, Sci. Bull. **63**, 1545 (2018).

[87] S.-J. Ran, B. Xi, C. Peng, G. Su, and M. Lewenstein, Phys. Rev. B **99**, 205132 (2019).

[88] B. Vanhecke, D. Devoogdt, F. Verstraete, and L. Vanderstraeten, arXiv:2112.01507.

[89] L. Wang and F. Verstraete, arXiv:1110.4362.

[90] M. Lubasch, J. I. Cirac, and M.-C. Bañuls, New J. Phys. **16**, 033014 (2014).

[91] M. Lubasch, J. I. Cirac, and M.-C. Bañuls, Phys. Rev. B **90**, 064425 (2014).

[92] D. Basko, I. Aleiner, and B. Altshuler, Ann. Phys. (NY) **321**, 1126 (2006).

[93] D. A. Abanin, E. Altman, I. Bloch, and M. Serbyn, Rev. Mod. Phys. **91**, 021001 (2019).

[94] A. Pal and D. A. Huse, Phys. Rev. B **82**, 174411 (2010).

[95] R. Vosk, D. A. Huse, and E. Altman, Phys. Rev. X **5**, 031032 (2015).

[96] M. Goihl, M. Gluza, C. Krumnow, and J. Eisert, Phys. Rev. B **97**, 134202 (2018).

[97] P. Bordia, H. Lüschen, S. Scherg, S. Gopalakrishnan, M. Knap, U. Schneider, and I. Bloch, Phys. Rev. X **7**, 041047 (2017).

[98] W. De Roeck and F. Huveneers, Phys. Rev. B **95**, 155129 (2017).

[99] A. Geißler and G. Pupillo, Phys. Rev. Res. **2**, 042037(R) (2020).

[100] T. B. Wahl, A. Pal, and S. H. Simon, Nat. Phys. **15**, 164 (2019).

[101] D. M. Kennes, arXiv:1811.04126.

[102] G. De Tomasi, F. Pollmann, and M. Heyl, Phys. Rev. B **99**, 241114(R) (2019).

[103] F. Andraschko, T. Enss, and J. Sirker, Phys. Rev. Lett. **113**, 217201 (2014).

[104] B. Paredes, F. Verstraete, and J. I. Cirac, Phys. Rev. Lett. **95**, 140501 (2005).

[105] F. Wilczek, Phys. Rev. Lett. **109**, 160401 (2012).

[106] H. Watanabe and M. Oshikawa, Phys. Rev. Lett. **114**, 251603 (2015).

[107] V. K. Kozin and O. Kyriienko, Phys. Rev. Lett. **123**, 210602 (2019).

[108] K. Sacha, Phys. Rev. A **91**, 033617 (2015).

[109] V. Khemani, A. Lazarides, R. Moessner, and S. L. Sondhi, Phys. Rev. Lett. **116**, 250401 (2016).

[110] D. V. Else, B. Bauer, and C. Nayak, Phys. Rev. Lett. **117**, 090402 (2016).

[111] N. Y. Yao, A. C. Potter, I.-D. Potirniche, and A. Vishwanath, Phys. Rev. Lett. **118**, 030401 (2017).

[112] J. Zhang, P. W. Hess, A. Kyprianidis, P. Becker, A. Lee, J. Smith, G. Pagano, I.-D. Potirniche, A. C. Potter, A. Vishwanath, N. Y. Yao, and C. Monroe, Nature (London) **543**, 217 (2017).

[113] S. Choi, J. Choi, R. Landig, G. Kucsko, H. Zhou, J. Isoya, F. Jelezko, S. Onoda, H. Sumiya, V. Khemani, C. von Keyserlingk, N. Y. Yao, E. Demler, and M. D. Lukin, Nature (London) **543**, 221 (2017).

[114] J. Rovny, R. L. Blum, and S. E. Barrett, Phys. Rev. Lett. **120**, 180603 (2018).

[115] S. Pal, N. Nishad, T. S. Mahesh, and G. J. Sreejith, Phys. Rev. Lett. **120**, 180602 (2018).

[116] J. Rovny, R. L. Blum, and S. E. Barrett, Phys. Rev. B **97**, 184301 (2018).

[117] J. Smits, L. Liao, H. T. C. Stoof, and P. van der Straten, Phys. Rev. Lett. **121**, 185301 (2018).

[118] L. Liao, J. Smits, P. van der Straten, and H. T. C. Stoof, Phys. Rev. A **99**, 013625 (2019).

[119] J. Smits, H. T. C. Stoof, and P. van der Straten, New J. Phys. **22**, 105001 (2020).

[120] K. Sacha and J. Zakrzewski, Rep. Prog. Phys. **81**, 016401 (2017).

[121] V. Khemani, R. Moessner, and S. L. Sondhi, arXiv:1910.10745.

[122] D. V. Else, C. Monroe, C. Nayak, and N. Y. Yao, Annu. Rev. Condens. Matter Phys. **11**, 467 (2020).

[123] P. Ponte, Z. Papić, F. Huveneers, and D. A. Abanin, Phys. Rev. Lett. **114**, 140401 (2015).

[124] A. Lazarides, A. Das, and R. Moessner, Phys. Rev. Lett. **115**, 030402 (2015).

[125] D. A. Abanin, W. De Roeck, and F. Huveneers, Ann. Phys. (NY) **372**, 1 (2016).

[126] T. Kuwahara, T. Mori, and K. Saito, Ann. Phys. (NY) **367**, 96 (2016).

[127] E. Canovi, M. Kollar, and M. Eckstein, Phys. Rev. E **93**, 012130 (2016).

[128] F. Machado, G. D. Kahanamoku-Meyer, D. V. Else, C. Nayak, and N. Y. Yao, Phys. Rev. Res. **1**, 033202 (2019).

[129] C. J. Turner, A. A. Michailidis, D. A. Abanin, M. Serbyn, and Z. Papić, Nat. Phys. **14**, 745 (2018).

[130] A. A. Michailidis, C. J. Turner, Z. Papić, D. A. Abanin, and M. Serbyn, Phys. Rev. X **10**, 011055 (2020).

[131] A. Pizzi, D. Malz, G. De Tomasi, J. Knolle, and A. Nunnenkamp, Phys. Rev. B **102**, 214207 (2020).

[132] F. M. Surace, M. Votto, E. G. Lazo, A. Silva, M. Dalmonte, and G. Giudici, Phys. Rev. B **103**, 104302 (2021).

[133] G. Evenbly, Phys. Rev. B **98**, 085155 (2018).